Published in Biochemistry, January 8, 1991, pp. 12–18, by the American Chemical Society

Four-Dimensional $^{13}C/^{13}C$-Edited Nuclear Overhauser Enhancement Spectroscopy of a Protein in Solution: Application to Interleukin 1β[†]

G. Marius Clore,* Lewis E. Kay, Ad Bax,* and Angela M. Gronenborn*

Laboratory of Chemical Physics, Building 2, National Institute of Diabetes and Digestive and Kidney Diseases, National Institutes of Health, Bethesda, Maryland 20892

Received September 18, 1990; Revised Manuscript Received October 24, 1990

ABSTRACT: A four-dimensional $^{13}C/^{13}C$-edited NOESY experiment is described which dramatically improves the resolution of protein NMR spectra and enables the straightforward assignment of nuclear Overhauser effects involving aliphatic and/or aromatic protons in larger proteins. The experiment is demonstrated for uniformly (>95%) ^{13}C-labeled interleukin 1β, a protein of 153 residues and 17.4 kDa, which plays a key role in the immune response. NOEs between aliphatic and/or aromatic protons are first spread out into a third dimension by the ^{13}C chemical shift of the carbon atom attached to the originating proton and subsequently into a fourth dimension by the ^{13}C chemical shift of the carbon atom attached to the destination proton. Thus, each NOE cross peak is labeled by four chemical shifts. By this means, ambiguities in the assignment of NOEs that arise from chemical shift overlap and degeneracy are completely removed. Further, NOEs between protons with the same chemical shifts can readily be detected providing their attached carbon atoms have different ^{13}C chemical shifts. The design of the pulse sequence requires special care to minimize the level of artifacts arising from undesired coherence transfer pathways, and in particular those associated with "diagonal" peaks which correspond to magnetization that has not been transferred from one proton to another. The 4D $^{13}C/^{13}C$-edited NOESY experiment is characterized by high sensitivity as the through-bond transfer steps involve the large $^1J_{CH}$ (130 Hz) couplings, and it is possible to obtain high-quality spectra on 1–2 mM samples of ^{13}C-labeled protein in as little as 3 days. This experiment should open up the application of protein structure determination by NMR to a large number of medium-sized proteins (150–300 residues) of biological interest.

The key to protein structure determination by NMR[1] spectroscopy lies in the identification of as many nuclear Overhauser effects (NOEs) as possible, which yield geometric information in the form of approximate interproton distance restraints (Wüthrich, 1986; Clore & Gronenborn, 1989). Over the last few years it has been convincingly demonstrated that solution structures comparable to 2–2.5 Å resolution X-ray structures can be obtained by NMR for proteins up to about 100 residues (Kline et al., 1988; Kraulis et al., 1989; Clore et al., 1990a; Qian et al., 1990; Omichinski et al., 1990; Dyson et al., 1990). This accuracy and precision depend critically on the number of NOEs that can be assigned (Clore & Gronenborn, 1991). As proteins get larger than about 120 residues (~13 kDa), resonance overlap and degeneracy are so extensive that it frequently becomes impossible to assign a large portion of the NOEs with any degree of confidence

[†] This work was supported by the AIDS-directed Anti-Viral Program of the Office of the Director of the National Institutes of Health (G.M.C., A.M.G., and A.B.). L.E.K. was supported by a postdoctoral Centennial Fellowship from the Medical Research Council of Canada.

[1] Abbreviations: NMR, nuclear magnetic resonance; NOE, nuclear Overhauser effect; NOESY, nuclear Overhauser enhancement spectroscopy; HMQC, heteronuclear multiple quantum coherence; IL-1β, interleukin 1β.

by conventional 2D NMR methodology (Driscoll et al., 1990a). This problem can be overcome in principle by increasing the dimensionality of the acquired spectra into a third dimension (Griesinger et al., 1987; Oschkinat et al., 1988; Vuister et al., 1988; Fesik & Zuiderweg, 1988, 1990; Marion et al., 1989a,b; Clore & Gronenborn, 1991). With the advent of 3D NMR, it has become possible to obtain complete ^1H, ^{15}N, and ^{13}C assignments of proteins in the range 15–20 kDa, as has been recently demonstrated in the case of interleukin 1β (IL-1β) (Driscoll et al., 1990a,b; Clore et al., 1990b), a protein of 153 residues and molecular mass 17.4 kDa, which plays a central role in the immune and inflammatory responses (Oppenheim et al., 1986; Arai et al., 1990). Nevertheless, although a fair number of NOEs between residues far apart in the sequence could be obtained by 3D ^{15}N- or ^{13}C-edited nuclear Overhauser enhancement (NOESY) spectroscopy, a larger number is still difficult to assign unambiguously owing to extensive spectral overlap. Indeed, in the case of our studies on IL-1β, we were unable to readily assign a large-enough number of NOEs in the 3D heteronuclear-edited NOESY spectra to allow the determination of a high-resolution structure of the quality now attainable for small proteins, although the information content was sufficient to obtain a low-resolution structure (Clore et al., 1990c). The potential solution to this impasse lies in extending the dimensionality of the NMR spectra still further. In this regard, we recently demonstrated the use of 4D $^{15}N/^{13}C$-edited NOESY spectroscopy to remove ambiguities in the assignment of NOEs between amide and carbon-attached protons (Kay et al., 1990a). The majority of NOEs in a protein, however, involve interactions between carbon-attached protons, and assigning all these interactions in the aliphatic region of the NOESY spectrum is frequently impossible. It therefore becomes essential for the structure determination of larger proteins to unravel and simplify this most crowded region of the NOESY spectrum. In this paper we show that 4D $^{13}C/^{13}C$-edited NOESY spectroscopy is an efficient and practical approach for attaining this goal, allowing the straightforward assignment of NOEs involving aliphatic and/or aromatic protons. The applicability of the method is demonstrated on uniformly (>95%) ^{13}C-labeled IL-1β.

Experimental Procedures

Recombinant human IL-1β was expressed in *Escherichia coli* and purified as described previously (Wingfield et al., 1986). Uniform ^{15}N and ^{13}C labeling to a level of >95% was obtained by growing the bacteria in minimal medium containing $^{15}NH_4Cl$ and [$^{13}C_6$]glucose as the sole nitrogen and carbon sources, respectively. The sample for the NMR experiment contained 1.7 mM $^{15}N/^{13}C$-labeled IL-1β in 90 mM sodium phosphate buffer, pH 5.4, dissolved in 99.996% D_2O.

All NMR spectra were recorded on a Bruker AM600 spectrometer equipped with an inverse probe.

The 4D spectrum was processed on a Sun Sparc workstation. The $F_2(^1H)$–$F_4(^1H)$ planes were processed with the commercially available software package NMR2 (New Methods Research, Inc., Syracuse, NY). The remaining processing was carried out with simple in-house routines (Kay et al., 1989) for the Fourier transforms in the $F_1(^{13}C)$ and $F_3(^{13}C)$ dimensions, the inverse Fourier transform in F_3, and the linear prediction in F_1 and F_3. The linear prediction singular value decomposition algorithm employed was derived from that of Barkhuijsen and de Beer (1985). A number of features specific to the present linear prediction algorithm are worth noting. First, as the data in the two ^{13}C dimensions (F_1 and F_3) are to be extended by a factor of 2, it is essential to treat the data as complex numbers (Kay et al., 1990b) rather than predicting the real and imaginary components separately (Olejniczak & Eaton, 1990). Second, it is necessary to use a process known as root reflection (Press et al., 1989) to ensure that the predicted part of the time domain does not increase in amplitude (Zhu & Bax, 1990), which involves calculating the roots of an nth-order polynomial, where n is the number of prediction coefficients. Third, the negative time behavior is calculated, giving a doubling of the size of the time domain data used as input for the linear prediction program (Zhu & Bax, 1990). This can be done as the sampling in the t_1 and t_3 dimensions is delayed by half a dwell time so that, neglecting signal decay and using the fact that at time zero the signal phase is zero, the data at negative time are the complex conjugates of the data recorded at positive time. Thus, for a data point x_n at positive time, the corresponding point at negative time is given by $x_{-n} = x_n^*$. While no additional signal is generated by this procedure, since the noise is correlated for both positive and negative time domain points, it does result in an increase by a factor of 2 in the number of time domain points which can be used for linear prediction, thereby effectively doubling the number of frequencies that can be extracted from the data. Thus, it allows as many as N frequency components to be determined, where N is the number of complex data points collected. In practice, for $2N$ (16) data points (including the negative time domain data) we use $K = N - 2$ (6) prediction coefficients, resulting in $N + 2$ (10) linear equations.

Table I: Flowchart of the Steps Used in Processing the 4D Data Set

step	calculation performed
1	Fourier transform in $t_3(^{13}C)$ dimension
2	processing of the $t_2(^1H)$–$t_4(^1H)$ planes
3	linear prediction of $t_1(^{13}C)$ time domain
4	processing of $t_1(^{13}C)$ dimension
5	inverse Fourier transform in $t_3(^{13}C)$
6	linear prediction of $t_3(^{13}C)$ time domain
7	processing of $t_3(^{13}C)$ dimension

The necessity to extend the severely truncated signals in t_1 and t_3 (only eight complex data points) by linear prediction in order to obtain reasonable digital resolution in the two ^{13}C dimensions entails the use of a more complex processing scheme than would otherwise be the case if conventional Fourier transformation only had been employed. Because the linear prediction is performed in one dimension at a time, the number of frequency components present in the time domain to be extended must be minimized. This is achieved by Fourier transformation in all the other dimensions prior to linear prediction of the dimension of interest (Schussheim & Cowburn, 1987). Thus, the t_3 dimension is transformed first, followed by processing of the t_2 and t_4 dimensions with appropriate digital filtering, zero filling, Fourier transformation, and phasing. The imaginary parts in F_2 and F_4 are discarded at the end of this stage. The t_1 dimension is then extended by linear prediction, followed by digital filtering, zero filling, Fourier transformation, and phasing. Subsequently, the imaginary parts in t_1 are discarded. Finally, the resolution in the t_3 dimension is increased by a process involving inverse Fourier transformation, followed by linear prediction, digital filtering, zero filling, forward Fourier transformation, and phasing in t_3. A flowchart for the processing of the 4D data is given in Table I.

Results and Discussion

Conceptually, the sequence for the new 4D $^{13}C/^{13}C$-edited NOESY experiment is analogous to that of the 4D $^{15}N/^{13}C$-edited one (Kay et al., 1990a). However, we found develop-

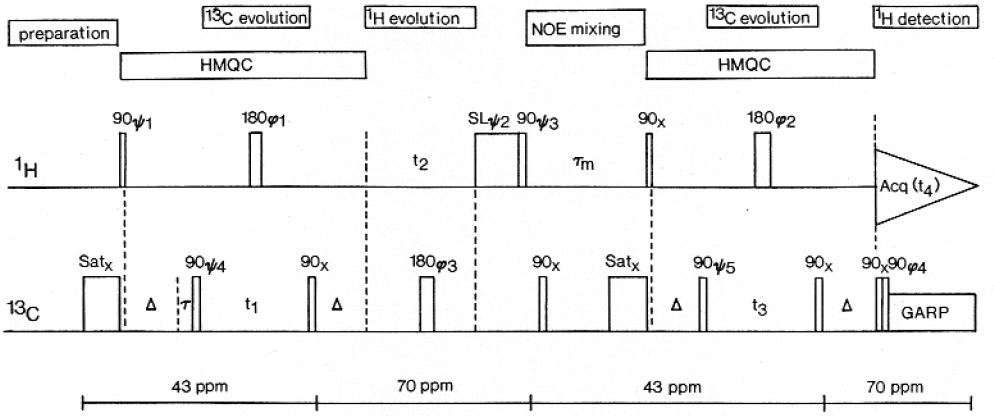

FIGURE 1: Pulse scheme for the 4D $^{13}C/^{13}C$-edited NOESY experiment. The ^{13}C 180° pulse is a composite pulse (90_x–180_y–90_x). The eight-step phase cycle is as follows: $\psi 1 = x; \psi 2 = -y; \psi 3 = x; \psi 4 = x, -x; \psi 5 = 2(x), 2(-x); \phi 1 = 4(x), 4(y); \phi 2 = 4(x), 4(y); \phi 3 = 2(x), 2(-x); \phi 4 = x, -x$; Receiver = $x, 2(-x), x$. The 1-ms ^{13}C saturation pulse (Sat_x) right at the beginning of the sequence prevents magnetization originating on ^{13}C spins from being transferred to coupled ^{1}H spins via a DEPT (Bendall et al., 1981) type mechanism. In the same vein, the ^{13}C 90_x pulse applied at the beginning of the NOESY mixing period converts all residual I_zS_z magnetization to I_zS_x, and longitudinal ^{13}C magnetization remaining at the end of the NOESY mixing period (τ_m) is removed by the second 1-ms ^{13}C saturation pulse (Sat_x). The ^{1}H spin lock pulse ($SL\psi 2$) along the $-y$ axis, which is applied for 500 μs prior to the second ^{1}H 90° pulse, ensures that all ^{1}H magnetization other than that lying along $-y$ is dephased. The delay Δ is set to $1/(2J_{CH})$ (~3.4 ms) to allow for efficient creation of ^{1}H–^{13}C multiple quantum coherence. The TPPI–States method (Marion et al., 1989c) is used to obtain quadrature in F_1, F_2, and F_3 with some minor modifications: after the eight-step phase cycle is completed $\psi 2$ and $\psi 3$ are decremented by 90° in concert for each t_1 value; $\psi 4$ and $\psi 5$ are incremented by 90° independently of each other, as well as of $\psi 2$ and $\psi 3$, for every t_2 and t_3 value, respectively; and data for $\psi 3 = x, -y, \psi 4 = x, y$, and $\psi 5 = x, y$ are stored separately to be processed as complex data. In addition, everytime t_1, t_2, and t_3 are incremented, $\psi 4$ and the receiver phase, $\psi 1$ and the receiver phase, and $\psi 5$ and the receiver phase, respectively, are also incremented by 180°. Thus, in the case of the t_2 dimension, the States part of the method for obtaining quadrature in the F_2 dimension is applied to $\psi 2$ and $\psi 3$, while the TPPI part is applied to $\psi 1$. The delay τ, immediately prior to the application of the first ^{13}C 90° pulse, is set to the duration of the ^{13}C 180° composite pulse. This serves to compensate for the ^{13}C 180° pulse in the middle of t_2 so that no first-order phase correction is necessary in F_2. The length of the initial t_1 and t_3 delays is adjusted to exactly half a dwell time such that the zero- and first-order phase corrections in F_1 and F_3 are 90° and −180°, respectively. This is achieved by setting $[t_{1,3}(0) + \tau_{180}(^{1}H) + 4\tau_{90}(^{13}C)/\pi] = \Delta t_{1,3}/2$, where $\Delta t_{1,3}$ is the value of the t_1 and t_3 increment and $t_{1,3}(0)$ is the initial value of the t_1 and t_3 delays. This ensures that the folded peaks are all absorptive and have positive or negative amplitudes depending on whether the number of times they are folded is even or odd, respectively (Bax et al., 1990a,b). It also permits one to extend the data to negative time as each negative time point x_{-n} is given by the complex conjugate of the corresponding positive time point x_n, thereby doubling the length of the time domain data in the F_1 and F_3 dimensions prior to linear prediction (Zhu & Bax, 1990). ^{13}C decoupling during acquisition is achieved with ^{13}C coherent GARP modulation (Shaka et al., 1985). The $90°_x$–$90°\pm_x$ ^{13}C pulse pair immediately prior to the start of GARP decoupling serves to reduce the intensity of modulation sidebands (Bax et al., 1990a). The ^{13}C carrier frequency was switched between 43 and 70 ppm several times during the sequence as indicated at the bottom of the figure, the former position being used during the evolution periods t_1 and t_3 and the latter for ^{13}C decoupling during t_2 and t_4. This ensures that the carbon frequency is centered in the middle of the ^{13}C chemical shift range for efficient ^{13}C decoupling. The ^{1}H carrier frequency was set to 3.5 ppm. In the spectrum presented in this paper, the NOE mixing time τ_m was set to 110 ms, and the relaxation delay was 0.9 s. Radio-frequency field strengths of 28.7, 15, and 3.9 kHz were used for the ^{1}H and ^{13}C pulses and for GARP decoupling, respectively. The acquired 3D data matrix comprised 8 complex (t_1) × 64 complex (t_2) × 8 complex (t_3) × 256 real (t_4) data points, and the total measuring time was 78 h. The spectral widths in F_1, F_2, F_3, and F_4 were 3125, 5263, 3125, and 5346 Hz, respectively, with corresponding acquisition times of 2.56, 12.16, 2.56, and 23.94 ms, respectively. The absorptive part of the final processed data matrix comprised 32 × 128 × 32 × 256 points with a digital resolution of 97.7, 41.1, 97.7, and 21 Hz in F_1, F_2, F_3, and F_4, respectively.

ment of a suitable scheme for obtaining artifact-free 4D $^{13}C/^{13}C$-edited NOESY spectra much more complicated than for the $^{15}N/^{13}C$-edited case. The increase in difficulty arises from the larger number of spurious magnetization transfer pathways that can lead to observable signals in the present homonuclear ^{13}C case. In addition, in the 4D $^{15}N/^{13}C$-edited case there are no "diagonal peaks" which would correspond to magnetization that has not been transferred from one hydrogen to another, as the double heteronuclear filtering is extremely efficient at completely removing these normally very intense uninformative resonances. In the present case it is not possible to use a similar procedure for suppressing these diagonal peaks, making it extremely hard to design a pulse sequence that minimizes the level of artifacts associated with these intense resonances. Thus, it was not clear a priori whether useful 4D $^{13}C/^{13}C$-edited NOESY spectra with adequate resolution and a sufficiently low level of artifacts could be obtained.

The pulse scheme for the 4D $^{13}C/^{13}C$-edited NOESY experiment shown in Figure 1 is the result of a long and iterative procedure. It comprises three parts with a central ^{1}H–^{1}H NOESY sequence between two ^{1}H–^{13}C heteronuclear multiple quantum coherence (HMQC; Mueller, 1979; Bax et al., 1983) sequences. Thus, transfer of magnetization follows the pathway

$$^{1}H \xrightarrow{^{1}J_{CH}} {}^{13}C \xrightarrow{^{1}J_{CH}} {}^{1}H \xrightarrow{NOE} {}^{1}H \xrightarrow{^{1}J_{CH}} {}^{13}C \xrightarrow{^{1}J_{CH}} {}^{1}H$$

and ^{1}H magnetization of the originating and destination protons evolves during the evolution period t_2 and the acquisition time t_4, respectively, while the corresponding ^{13}C chemical shifts of the directly bonded carbon atoms evolve during the evolution periods t_1 and t_3. To obtain a satisfactory level of artifact suppression, we found it necessary to use phase cycling for eight of the radio-frequency pulses shown in the pulse scheme depicted in Figure 1. By executing noninteracting phase cycles in a concomitant fashion (Bax et al., 1990a), we were able to conduct all the phase cycling in eight steps. Details regarding the logic behind the choice of the combination of phase cycles employed will be presented elsewhere.

With a minimum of eight scans per (t_1, t_2, t_3) increment, the maximum number of increments that can be obtained in a few days worth of measuring time is severely restricted. We chose to use 256 real points in the t_4 (^{1}H) acquisition dimension, 64 complex points in the t_2 (^{1}H) dimension, and only

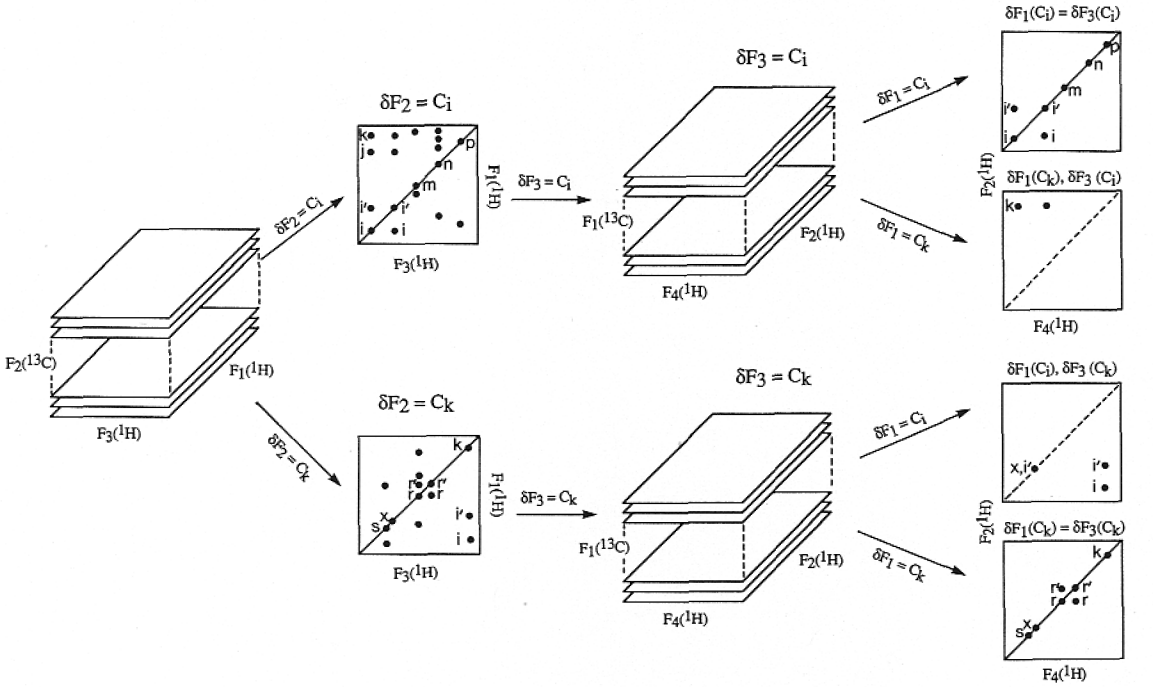

3D 3D $F_1(^1H)$-$F_3(^1H)$ planes 4D $F_1(^{13}C)$,$F_2(^1H)$,$F_4(^1H)$ cubes 4D $F_2(^1H)$-$F_4(^1H)$ planes

FIGURE 2: Schematic representation of the relationship between 3D ^{13}C-edited NOESY and 4D $^{13}C/^{13}C$-edited NOESY spectra. In the example illustrated in this figure we consider three protons close in space comprising the methylene protons i and i' attached to the same carbon atom C_i and a methyl proton k attached to the carbon atom C_k. In the 3D spectrum, the diagonal peaks for the methylene protons i and i' and NOE cross peaks between the methylene protons i and i' and from the methyl proton k to the methylene protons i and i' are seen at the $^{13}C(F_2)$ frequency of C_i; the diagonal peak for k and the NOEs from i and i' to k are seen at the $^{13}C(F_2)$ frequency of C_k. In the 4D spectrum, the diagonal peaks for the methylene protons i and i' and the methyl proton k are seen in the $^1H(F_2)$–$^1H(F_4)$ planes at $\delta F_1(^{13}C_i) = \delta F_3(^{13}C_i)$ and $\delta F_1(^{13}C_k)$, respectively. The NOEs from k to i are seen in the $^1H(F_2)$–$^1H(F_4)$ plane at $\delta F_1(C_k)$, $\delta F_3(C_i)$, while the NOEs from i and i' and k are seen in the $^1H(F_2)$–$^1H(F_4)$ planes at $\delta F_1(C_i)$, $\delta F_3(C_k)$. Also shown in the latter plane is an NOE between two protons x and i' with identical chemical shifts, where the chemical shift of the carbon atom attached to x is the same as that of C_k.

8 complex points in the t_1 and t_3 (^{13}C) dimensions. However, the use of extensive folding in the ^{13}C dimensions (Kay et al., 1989; Bax et al., 1990a,b; Clore et al., 1990), combined with the use of an improved linear prediction procedure (Zhu & Bax, 1990), resulted in acceptable resolution in these dimensions. As indicated under Experimental Procedures, the latter uses prior knowledge regarding both the phase of the signal at $t_1 = 0$ and $t_3 = 0$ and the damping factor in the severely truncated time dimensions, thus enabling more accurate determination of the remaining unknowns comprising the frequency and amplitude of each signal component.

The complete 4D spectrum was recorded in only 78 h on a 1.7 mM uniformly (>95%) $^{13}C/^{15}N$-labeled sample of IL-1β. The F_1 and F_3 dimensions were extended to 16 complex points by the modified linear prediction procedure mentioned above, and zero filling in all dimensions resulted in a 32 × 128 × 32 × 256 data point matrix for the fully processed absorptive portion of the spectrum.

The relationship between 3D ^{13}C-edited NOESY and 4D $^{13}C/^{13}C$-edited NOESY spectra is shown in Figure 2. The 3D spectrum comprises a single cube in which NOEs appear in different ^1H–^1H planes determined by the ^{13}C chemical shift of the carbon atom attached to the destination proton. Each ^1H–^1H slice of the 3D cube constitutes a cube in the 4D spectrum in which the NOEs are further edited by the ^{13}C chemical shift of the carbon atom bonded to the originating proton. Thus, the 4D spectrum consists of a series of 3D cubes at different ^{13}C chemical shifts in the F_3 dimension, corresponding to the resonance frequency of the carbon atom directly bonded to the destination proton(s), and the axes of each cube are the ^1H chemical shifts of the originating and destination protons in F_2 and F_4, respectively, and the ^{13}C chemical shift of the carbon atom attached to the originating proton in the F_1 dimension.

In principle, a 3D ^{13}C-edited NOESY spectrum (Ikura et al., 1990; Zuiderweg et al., 1990) contains approximately the same information as the 4D $^{13}C/^{13}C$-edited spectrum. However, in any given ^{13}C slice of the 3D spectrum, the NOE peak between the originating proton H_k and the destination proton H_i is only labeled by the two ^1H chemical shifts and the ^{13}C chemical shift of the carbon atom directly bonded to the destination proton C_i. In the majority of cases there are many protons which resonate at the same ^1H chemical shift as H_k. Consequently, in the 3D spectrum it is essential to be able to locate the symmetry-related NOE cross peak at the ^{13}C chemical shift of the carbon atom C_k directly bonded to H_k in order to assign the identity of H_k with any degree of confidence. This task is rendered difficult due to the presence of t_1 noise and extensive spectral overlap in the ^1H (F_1) dimension, as well as by the fact that many of the NOE peaks are of very weak intensity and may not appear in both locations in the 3D spectrum. In the case of the 4D spectrum, all this information is contained in a single peak. Further, each NOE appears twice in the 4D spectrum (as the ^{13}C shifts of the destination and originating carbon atoms are swapped), providing a means to improve the quality of the spectrum by symmetrization. An additional and major advantage of the 4D over the 3D spectrum is that in the 4D spectrum genuine "diagonal" peaks corresponding to magnetization that has not been transferred from one proton to another, as well as the

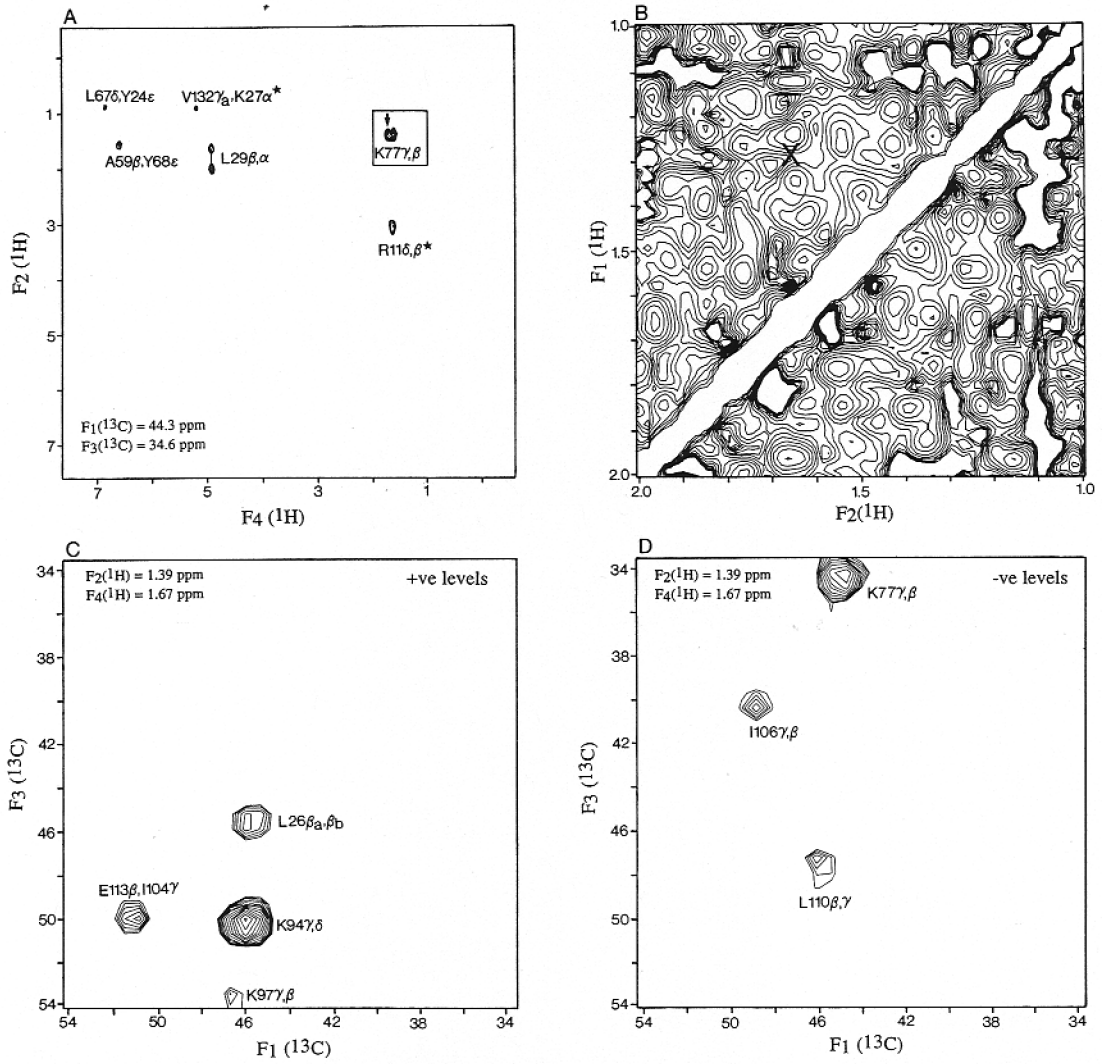

FIGURE 3: Selected $F_2(^1H)$–$F_4(^1H)$ and $F_1(^{13}C)$–$F_3(^{13}C)$ planes of the 4D $^{13}C/^{13}C$-edited NOESY spectrum of 1.7 mM uniformly (>95%) $^{13}C/^{15}N$-labeled IL-1β recorded on a Bruker AM600 spectrometer. (A) $F_2(^1H)$–$F_4(^1H)$ slice at $\delta F_1(^{13}C)$ = 44.3 ppm and $\delta F_3(^{13}C)$ = 34.6 ppm; (C and D) positive and negative contours of the $F_1(^1H)$–$F_3(^{13}C)$ plane at $\delta F_2(^1H)$ = 1.39 ppm, $\delta F_4(^1H)$ = 1.67 ppm corresponding to the ^1H chemical shifts of the cross peak between the C$^{\gamma}$H and C$^{\beta a}$H protons of Lys-77 shown by the arrow in (A); (B) region between 1 and 2 ppm of the 110-ms 2D NOESY spectrum of IL-1β (with a digital resolution of 6.9 Hz), corresponding to the boxed region shown in (A). [The X marks the ^1H coordinates of the peak indicated by the arrow in (A).] Note that because extensive folding is employed, the ^{13}C chemical shifts are given by $x \pm n$SW, where x is the ppm value listed in the figure, n is an integer, and SW is the spectral width (20.71 ppm). In (A) there are two positive cross peaks indicated by an asterisk, while the remaining cross peaks are negative. In the peak assignments, the first proton refers to the originating proton, while the second relates to the destination one. It should also be noted that small differences in ^{13}C chemical shifts (up to half a data point ~0.4 ppm) with values reported earlier (Clore et al., 1990b) are caused by the software used for peak picking of poorly digitized spectra in the earlier work.

intense NOE peaks involving protons attached to the same carbon atom (i.e., methylene protons), appear in only a single $F_2(^1H)$–$F_4(^1H)$ plane of each $F_1(^{13}C)$,$F_2(^1H)$,$F_4(^1H)$ cube at the carbon frequency where the originating and destination carbon atoms coincide (i.e., at $F_1 = F_3$). Therefore, these intense resonances no longer obscure NOEs between protons with similar or even degenerate chemical shifts, thus providing additional valuable interproton distance restraints for the 3D structure determination.

Examples of several $F_2(^1H)$–$F_4(^1H)$ and $F_1(^{13}C)$–$F_3(^{13}C)$ planes of the 4D $^{13}C/^{13}C$-edited NOESY spectrum of IL-1β recorded with a 110-ms mixing time are shown in Figures 3 and 4, which clearly reveal their extreme simplicity. Of particular importance is that the total number of cross peaks in the spectrum remains constant as the dimensionality, and concomitantly the spectral resolution, is increased. Note that the signal-to-noise ratio is excellent as the through-bond transfer steps are highly efficient due to the large $^1J_{CH}$ couplings (~130 Hz). Consequently, the experiment is much less sensitive to wide line widths associated with larger proteins. Indeed, all the cross peaks seen in the 3D ^{13}C-edited NOESY spectrum are also observed in the 4D one. Interpretation of the complete 4D spectrum is straightforward with a simple search algorithm to match up the four chemical shift coordinates of each peak with the complete list of ^1H and ^{13}C assignments already available (Clore et al., 1990b).

Figure 3A shows the $F_2(^1H)$–$F_4(^1H)$ plane at $\delta F_1(^{13}C)$, $\delta F_3(^{13}C)$ = 44.3, 34.6 ppm. (Note that because of extensive folding each ^{13}C frequency corresponds to several ^{13}C chemical shifts given by $x \pm n$SW, where x is the shift specified, n an integer, and SW the spectral width of 20.71 ppm.) A number of long-range NOE cross peaks are clearly discerned involving both aromatic and aliphatic protons. In addition, there are a number of intraresidue cross peaks. The intraresidue NOE between the C$^{\beta}$H and C$^{\gamma}$H protons of Lys-77 occurs in the region between 1 and 2 ppm. A plot of this region of the 2D spectrum is shown in Figure 3B, and the position of the peak between the C$^{\gamma}$H and C$^{\beta a}$H protons of Lys-77, which is in-

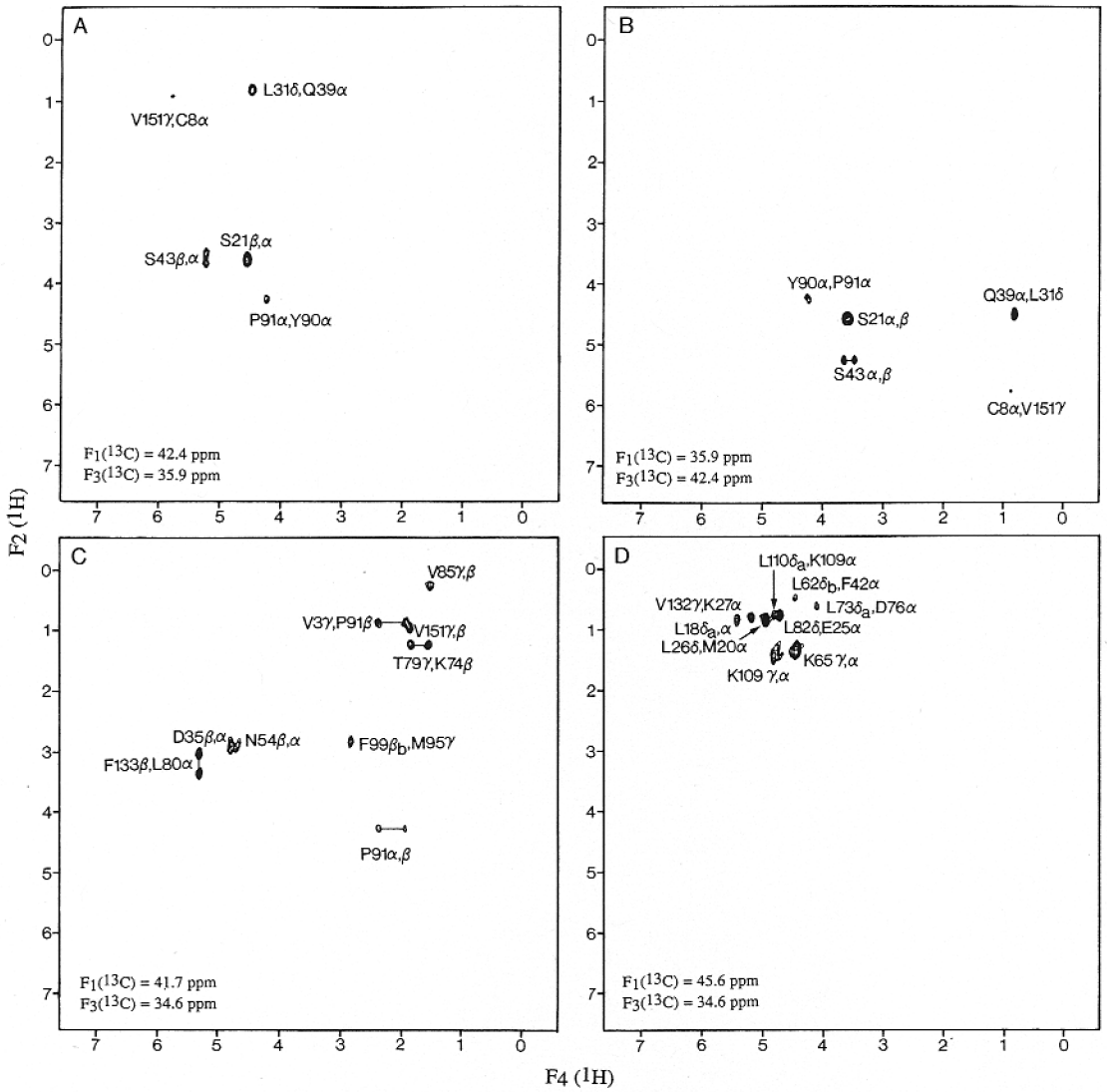

FIGURE 4: Selected $F_2(^1H)$–$F_4(^1H)$ slices at several $F_3(^{13}C)$ and $F_1(^{13}C)$ chemical shifts of the 4D $^{13}C/^{13}C$-edited NOESY spectrum of IL-1β. (A and B) "Mirror image" planes displaying NOE interactions between the same set of protons. (C and D) Two ^1H–^1H planes taken at the same $F_3(^{13}C)$ frequency but different $F_1(^{13}C)$ frequencies. A single slice of a regular 3D ^{13}C-edited NOESY spectrum in the present case would consist of 32 such planes superimposed on one another. Only positive contours are displayed in (A), (B), and (C), while only negative ones are plotted in (D). In the peak assignments, the first proton refers to the originating proton, while the second relates to the destination one.

dicated by the arrow in Figure 3A, is marked by the letter X in Figure 3B. It is clear from Figure 3B that no individual cross peaks can be resolved in this region of the 2D spectrum. Panels C and D of Figure 3 show the positive and negative contours, respectively, of the $F_1(^{13}C)$–$F_3(^{13}C)$ plane at $\delta F_2(^1H)$, $\delta F_4(^1H)$ = 1.39, 1.67 ppm corresponding to the ^1H coordinates of the cross peak between the $C^\gamma H$ and $C^{\beta a}H$ protons of Lys-77. Four positive cross peaks (in which the number of times the peaks are folded is even) and three negative ones (in which the number of times the peaks are folded is odd) are clearly resolved in this single $F_1(^{13}C)$–$F_3(^{13}C)$ plane of the spectrum. Thus, seven NOE cross peaks are superimposed at the ^1H coordinates of 1.39, 1.67 ppm. Of these seven cross peaks, six involve intraresidue NOEs between protons separated by three bonds, which are of little structural value. However, the seventh is an interresidue NOE between the $C^\beta H$ proton of Glu-113 and the $C^\gamma H$ protons of Ile-104, which could not have been assigned in either a 2D or a 3D ^{13}C-edited NOESY spectrum.

Panels A and B of Figure 4 show two $F_2(^1H)$–$F_4(^1H)$ planes at $\delta F_1(^{13}C)$, $\delta F_3(^{13}C)$ = 42.4, 35.9 ppm and 35.9, 42.4 ppm, respectively. Thus, these two planes are related by symmetry, and the same NOEs are observed with comparable intensities in both planes with the $F_2(^1H)$ and $F_4(^1H)$ frequencies of the cross peaks interchanged. There are two intraresidue NOEs involving the $C^\alpha H$ and $C^\beta H$ protons of Ser-21 and Ser-43, and two long-range interresidue NOEs between Cys-8($C^\alpha H$) and Val-151($C^\gamma H_3$) and between Gln-39($C^\alpha H$) and Leu-31($C^\delta H_3$). In addition, there is a sequential NOE between the $C^\alpha H$ protons of Tyr-90 and Pro-91, indicative of a *cis*-proline. Of particular interest is that this NOE involves two protons with nearly identical chemical shifts (4.19 and 4.25 ppm for Tyr-90 and Pro-91, respectively) which would have been very difficult to observe in either a 2D spectrum or a 3D ^{13}C-edited NOESY spectrum, as the cross peak is located very close to the diagonal.

Panels C and D of Figure 4 illustrate two $F_2(^1H)$–$F_4(^1H)$ planes at one $F_3(^{13}C)$ chemical shift and two $F_1(^{13}C)$ chemical shifts. Both intraresidue and long-range interresidue NOE cross peaks are clearly observed and readily assigned. Also seen in Figure 4C is another NOE between two protons with near degenerate chemical shifts, namely, the NOE between Phe-99($C^{\beta b}H$) and Met-95($C^\gamma H$) at $\delta F_2(^1H)$, $\delta F_4(^1H)$ = 2.87, 2.75 ppm. Moreover, the digital resolution in the ^1H dimensions is sufficient to even resolve NOEs in crowded regions

of the spectrum such as that presented in Figure 4D between 0.5 and 1 ppm in F_2 and 4 and 5.5 ppm in F_4 which displays a number of NOEs from methyl groups of Leu and Val, as well as $C^{\gamma}H$ protons of Lys, to $C^{\alpha}H$ protons.

Concluding Remarks

The 4D $^{13}C/^{13}C$-edited NOESY experiment described in this paper together with the previously described 4D $^{15}N/^{13}C$-edited NOESY experiment (Kay et al., 1990a) should permit the virtually automated assignment of NOEs in proteins up to 25 kDa once a complete set of ^{1}H, ^{15}N, and ^{13}C resonance assignments has been obtained by a variety of 3D double- and triple-resonance experiments. Analysis of the present spectrum suggests that problems of chemical shift overlap, which obscure the interpretation of NOE cross peaks, should be almost completely eliminated for proteins up to approximately 300 residues, thus opening the application of protein structure determination by NMR to a large number of medium-size proteins of biological interest. In this regard, it is worth emphasizing that provided uniformly ^{13}C- and ^{15}N-labeled protein can be obtained, recording such heteronuclear-edited 4D NOESY spectra is imminently practicable and high-quality 4D spectra can be obtained on relatively dilute samples (1–2 mM) in as little as 3 days.

Acknowledgments

We thank Dr. Paul Wingfield for preparing the sample of $^{13}C/^{15}N$-labeled interleukin 1β, Guang Zhu for help in the development of the linear prediction software, and Rolf Tschudin for valuable technical assistance.

References

Arai, K., Lee, F., Miyajuina, A., Miyatake, S., Arai, N., & Yokata, T. (1990) *Annu. Rev. Biochem. 59*, 783–836.

Barkhuijsen, H., de Beer, R., Bovee, W. M. M. J., & van Ormondt, D. (1985) *J. Magn. Reson. 61*, 465–481.

Bax, A., Griffey, R. H., & Hawkins, B. L. (1983) *J. Magn. Reson. 55*, 301–315.

Bax, A., Clore, G. M., Driscoll, P. C., Gronenborn, A. M., Ikura, M., & Kay, L. E. (1990a) *J. Magn. Reson. 87*, 620–627.

Bax, A., Ikura, M., Kay, L. E., & Zhu, G. (1990b) *J. Magn. Reson.* (in press).

Bendall, M. R., Doddrell, D. M., & Pegg, D. T. (1981) *J. Am. Chem. Soc. 103*, 4603–4605.

Clore, G. M., & Gronenborn, A. M. (1989) *CRC Crit. Rev. Biochem. Mol. Biol. 24*, 479–564.

Clore, G. M., & Gronenborn, A. M. (1991) *Annu. Rev. Biophys. Biophys. Chem. 20*, 29–63.

Clore, G. M., Appella, E., Yamada, M., Matsushima, K., & Gronenborn, A. M. (1990a) *Biochemistry 29*, 1689–1696.

Clore, G. M., Bax, A., Driscoll, P. C., Wingfield, P. T., & Gronenborn, A. M. (1990b) *Biochemistry 29*, 8172–8184.

Clore, G. M., Driscoll, P. C., Wingfield, P. T., & Gronenborn, A. M. (1990c) *J. Mol. Biol. 214*, 811–817.

Driscoll, P. C., Clore, G. M., Marion, D., Wingfield, P. T., & Gronenborn, A. M. (1990a) *Biochemistry 29*, 3542–3556.

Driscoll, P. C., Gronenborn, A. M., Wingfield, P. T., & Clore, G. M. (1990b) *Biochemistry 29*, 4668–4682.

Dyson, H. J., Gippert, G. P., Case, D. A., Holmgren, A., & Wright, P. (1990) *Biochemistry 29*, 4129–4136.

Fesik, S. P., & Zuiderweg, E. R. P. (1988) *J. Magn. Reson. 78*, 588–593.

Fesik, S. W., & Zuiderweg, E. R. P. (1990) *Q. Rev. Biophys. 23*, 97–131.

Griesinger, C., Sørensen, O. W., & Ernst, R. R. (1987) *J. Magn. Reson. 73*, 574–579.

Ikura, M., Kay, L. E., Tschudin, R., & Bax, A. (1990) *J. Magn. Reson. 86*, 204–209.

Kay, L. E., Marion, D., & Bax, A. (1989) *J. Magn. Reson. 84*, 72–84.

Kay, L. E., Clore, G. M., Bax, A., & Gronenborn, A. M. (1990a) *Science 249*, 411–414.

Kay, L. E., Ikura, M., Zhu, G., & Bax, A. (1990b) *J. Magn. Reson.* (in press).

Kline, A. D., Braun, W., & Wüthrich, K. (1988) *J. Mol. Biol. 204*, 675–724.

Kraulis, P. J., Clore, G. M., Nilges, M., Jones, T. A., Pettersson, G., Knowles, J., & Gronenborn, A. M. (1989) *Biochemistry 28*, 7241–7257.

Marion, D., Kay, L. E., Sparks, S. W., Torchia, D. A., & Bax, A. (1989a) *J. Am. Chem. Soc. 111*, 1515–1517.

Marion, D., Driscoll, P. C., Kay, L. E., Wingfield, P. T., Bax, A., Gronenborn, A. M., & Clore, G. M. (1989b) *Biochemistry 28*, 6150–6156.

Marion, D., Ikura, M., Tschudin, R., & Bax, A. (1989c) *J. Magn. Reson. 85*, 393–399.

Mueller, L. (1979) *J. Am. Chem. Soc. 101*, 4481–4484.

Omichinski, J., Clore, G. M., Appella, E., Sagakuchi, K., & Gronenborn, A. M. (1990) *Biochemistry 29*, 9324–9334.

Olejniczak, E. T., & Eaton, H. L. (1990) *J. Magn. Reson. 87*, 628–632.

Oppenheim, J. J., Kovacs, E. J., Matsushima, K., & Durum, S. K. (1986) *Immunol. Today 7*, 45–56.

Oschkinat, H., Griesinger, C., Kraulis, P. J., Søorensen, O. W., Ernst, R. R., Gronenborn, A. M., & Clore, G. M. (1988) *Nature 332*, 374–377.

Press, W. H., Flannery, B. P., Teukolsky, S. A., & Vetterling, W. T. (1989) in *Numerical Recipes in C: The Art of Scientific Computing*, pp 463–466, Cambridge University Press, Cambridge.

Qian, Y. Q., Billeter, M., Otting, G., Müller, M., Gehring, W. J., & Wüthrich, K. (1989) *Cell 59*, 573–580.

Schussheim, A. E., & Cowburn, D. (1987) *J. Magn. Reson. 71*, 371–378.

Shaka, A. J., Barker, P. B., & Freeman, R. (1985) *J. Magn. Reson. 64*, 547–552.

Vuister, G. W., Boelens, R., & Kaptein, R. (1988) *J. Magn. Reson. 80*, 176–185.

Wingfield, P. T., Payton, M., Tavernier, J., Barnes, M., Shaw, A., Rose, K., Simona, M. G., Demaczuk, S., Williamson, K., & Dayer, J.-M. (1986) *Eur. J. Biochem. 160*, 491–497.

Wüthrich, K. (1986) *NMR of Proteins and Nucleic Acids*, Wiley, New York.

Zhu, G., & Bax, A. (1990) *J. Magn. Reson.* (in press).

Zuiderweg, E. R. P., McIntosh, L. P., Dahlquist, F. W., & Fesik, S. W. (1990) *J. Magn. Reson. 86*, 210–216.